



Magnetic carbon nanotubes camouflaged with cell membrane as a drug discovery platform for selective extraction of bioactive compounds from natural products

Qi Hu^{a,b}, Yusi Bu^{a,b}, Xueyan Zhen^{a,b}, Ke Xu^{a,b}, Ruifang Ke^{a,b}, Xiaoyu Xie^{a,b,*}, Sicen Wang^{a,b,*}

^a School of Pharmacy, Health Science Center, Xi'an Jiaotong University, Xi'an 710061, China

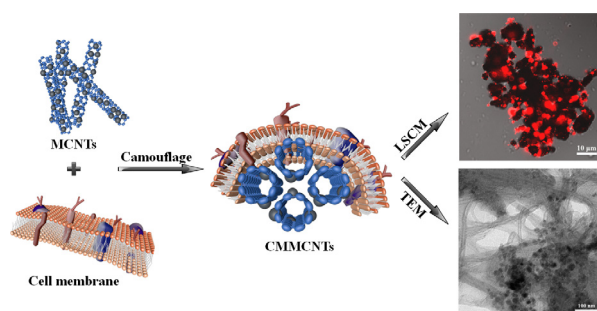
^b Shaanxi Engineering Research Center of Cardiovascular Drugs Screening & Analysis, Xi'an 710061, China



HIGHLIGHTS

- A novel cell membrane biomimetic CNTs nanosystem was first established.
- The resultant material had a right-side-out membrane and desired magnetic property.
- This successful application of material showed significant advantages in drug discovery.
- The cell membrane biomimetic modification could be widely used to improve the performance of CNTs in various applications.

GRAPHICAL ABSTRACT



ARTICLE INFO

Keywords:

Magnetic carbon nanotubes
Cell membrane-biomimetic functionalization
Receptor-ligand interaction
Drug discovery
TCM bioactive compounds screening

ABSTRACT

The biomimetic functionalization of carbon nanotubes (CNTs) are promising for its application in solid phase extraction because they can overcome current limitations of covalent functionalization and obtain desired specific recognition ability. The present study aimed to develop a novel dual functionalization CNTs modified with magnetic nanoparticles and high α_{1A} -adrenergic receptor (α_{1A} -AR) expression HEK 293 cell membrane. On the basis of the specific interactions between drugs and receptors on cell membrane, high α_{1A} -AR expression cell membrane camouflaged magnetic CNTs (CMMCNTs) were employed as a drug discovery platform to screen potential α_{1A} -AR antagonists from traditional Chinese medicine (TCM). The resultant CMMCNTs had a right-side-out membrane and desired magnetic property, enabling to rapidly target and separate the bioactive compounds from complex samples. Furthermore, the CMMCNTs possessed high adsorption capacity, fast binding kinetics, and satisfactory selectivity. As a result, two bioactive compounds as lappaconitine and benzoylmesaconine were screened and identified in the actual application. Moreover, the lappaconitine was validated to have favorable antagonism to α_{1A} -AR through preliminary pharmacological assays. Hence, this successful application of CMMCNTs showed significant advantages in drug discovery so as to drive the development of TCM. More importantly, the cell membrane biomimetic modification could be widely used to improve the performance of CNTs in various applications.

* Corresponding authors at: School of Pharmacy, Health Science Center, Xi'an Jiaotong University, Xi'an 710061, China.
E-mail addresses: xiexiaoyu@xjtu.edu.cn (X. Xie), wangsc@mail.xjtu.edu.cn (S. Wang).

<https://doi.org/10.1016/j.cej.2019.01.171>

Received 26 November 2018; Received in revised form 14 January 2019; Accepted 29 January 2019

Available online 30 January 2019

1385-8947/ © 2019 Elsevier B.V. All rights reserved.

1. Introduction

As promising nanomaterials, carbon nanotubes (CNTs) with its unique structure and properties has been widely used in various applications, including sample pretreatment [1], energy storage [2], sensing [3], biomedicine [4], etc. In the field of solid phase extraction (SPE), CNTs with an extremely large surface area has been developed as a considerable platform for the adsorption of a wide variety of organic and inorganic species [5]. For detecting the trace analytes from complex matrices, various functional modification methods for CNTs have been developed. Based on the special magnetic features of magnetic particles [6,7], one approach was to properly design the magnetic CNTs (MCNTs) composites, providing effective and powerful separation procedure [8,9]. Another way to improve the detection intensity was accomplished by chemical structure modification of CNTs, that was the grafting of desired functional groups on CNTs surface for enhancing the adsorption and dispersion ability [10,11]. However, the most commonly used methods of organic covalent modification, such as traditional acid modification and oxidation, have been reported to damage the intrinsic properties of CNTs [12,13], limiting their wider application.

Recently, the non-covalent modification for CNTs has been developed because these approaches could improve biocompatibility of CNTs and obtain desired binding interactions with targets, without compromising the physical properties [14,15]. For example, fungal mycelium was used to modify CNTs by a biological assembly approach to prepare adsorbents for water pollution control [16]. Biomimetic nanoparticles modified with active cell membrane have attracted widely attention [17,18]. By directly leveraging naturally derived cell membranes, this top-down method bestows nanoparticles with enhanced biointerfacing capabilities. This bionic functionalization was able to retain the complexity of the cell membrane, enabling the resultant membrane-camouflaged nanoparticles to take on many of the properties exhibited by the source cell [19,20]. Prior studies have shown utility of different cell membrane-cloaked nanoparticles with excellent features and functions in targeting virus [21], drug delivery [22], biodetoxification [23], and cancer therapy [24]. Inspired by this, by incorporating cell membrane onto CNTs, a novel cell-membrane-cloaked CNTs bionic material with more ligand recognition sites exhibited great potential in biological recognition.

Traditional Chinese medicine (TCM) is one of the most important resources of therapeutic agents [25]. Numerous active components screened from TCM, such as taxol [26] and camptothecin [27], have been developed into effective drugs to treat cancer. However, the classical methods for screening active ingredients started from the separation and purification of the single compound from complex TCM extracts, followed by biological validation of each purified compound in sequence [28], which were proved to be time-consuming and strenuous, and often miss the low-level compounds. Hence, developing more powerful screening tools for the bioactive ingredients of TCM is of great concern. As a major biological interface, the specific receptors in pharmaceutical-target interactions make cell membrane a promising tool for drug discovery [29–32]. Therefore, the cell membrane-cloaked CNTs exhibited great potential to target specific compounds acting on the cell membrane receptors from nature products.

In this study, a novel cell membrane-coated CNTs platform was established and applied to target and separate the potential bioactive compounds from TCM. α_{1A} -Adrenergic receptor (α_{1A} -AR) is a member of the G protein-coupled receptor superfamily [33], and has been proved to be effective drug targets for drug discovery [34]. Indeed, previous studies demonstrated that α_{1A} -AR has a close association with benign prostatic hyperplasia [35]. Therefore, high α_{1A} -AR expression HEK 293 cell membrane was herein used for CNTs functionalization to screen potential α_{1A} -AR antagonists. Moreover, based on the mature technology of magnetic functionality, magnetic nanoparticles were introduced onto the surface of CNTs via the in-situ reaction [36] to

achieve rapid magnetic separation. The characterization, adsorption properties, extraction conditions, and reproducibility of the resultant high α_{1A} -AR expression cell membrane-camouflaged magnetic CNTs (CMMCNTs) were systematically investigated. Furthermore, the antagonistic activity of the screened potential active compounds against α_{1A} -AR was further validated by pharmacological experiments. Such biomimetic cell membrane functionalization represents a new approach of CNTs modification, which improves the ability of targeting recognition while maintaining the original structure of the CNTs. Moreover, this biomimetic drug screening platform is expected to open the door for rapid targeting and separating bioactive ingredients in drug discovery.

2. Experiment section

2.1. Materials and reagents

Iron (III) chloride hexahydrate ($\text{FeCl}_3 \cdot 6\text{H}_2\text{O}$), iron (II) sulfate heptahydrate ($\text{FeSO}_4 \cdot 7\text{H}_2\text{O}$), ammonia solution (25% NH_3), and ethanol were obtained from Guanghua Technology Co., Ltd (Guangdong, China). Hydroxylated CNTs (CNTs-OH) (purity > 95%; length, 0.5–2 μm ; OD, 20–30 nm) was provided by XFNANO material technology Co., Ltd (Jiangsu, China). Lappaconite and benzoylmesaconine were obtained from Herbest Biological Technology (Shaanxi, China). Tamsulosin, silodosin, nitrendipine, metoprolol, and verapamil were purchased from Nanjing Ange Pharmaceutical Co., Ltd (Jiangsu, China). Methanol (HPLC-grade) was purchased from Thermo Fisher Scientific (Pittsburgh, USA). *Radix Aconiti* (RA) was obtained from the Xi'an medicine market (Shaanxi, China). Dulbecco's modified eagle medium (DMEM) and trypsin were obtained from Sigma-Aldrich LLC (Saint Louis, USA). 1,1'-Dioctadecyl-3,3,3',3'-tetramethylindocarbocyanine perchlorate (DiI) was purchased from Beyotime Bio. Tech. Co., Ltd (Shanghai, China). Ultra-pure water system was purchased by Feixiang Science Technology Co., Ltd (Beijing, China).

Standard stock solutions of tamsulosin, silodosin, nitrendipine, metoprolol, verapamil, lappaconitine, and benzoylmesaconine (1 mg mL^{-1}) were prepared in methanol, respectively. All solutions were prepared weekly and stored in the dark at 4 °C.

2.2. Instrumentation

The morphologies of obtained composites were observed by transmission electron microscopy (TEM; JEOL JEM-2100HR; Tokyo, Japan). Laser scanning confocal microscopy (LSCM) images were obtained using a TCS SP5 confocal microscope (Leica, Wetzlar, Germany) with a 549 nm solid state laser light source. Magnetic properties were determined with a Lake Shore 7307 vibrating sample magnetometer (VSM; Ohio, USA). Fourier transform infrared spectroscopy (FTIR) spectra were investigated by a Nicolet Nexus-410 FTIR spectrometer (Madison, USA) over a range of 4000–400 cm^{-1} . The elemental composition of the materials was performed with x-ray photoelectron spectroscopy (XPS) using Thermo Fisher K-Alpha XPS system (Pittsburgh, USA). The x-ray diffraction (XRD) patterns were recorded on a Bruker XRD equipped with $\text{Cu K}\alpha$ radiation over the range of $2\theta = 20 - 70^\circ$ (Bremen, Germany). Thermal gravimetric analysis (TGA) was measured from room temperature to 800 °C at a heating rate of 10 °C min^{-1} in air (STA 449 F3 Jupiter; Selb, Germany).

The HPLC/MS system consisted of SPD-M20A diode array detector and TOFMS system (Shimadzu Corporation, Kyoto, Japan). A reversed phase Inertsil/WondaSil C_{18} column (150 mm \times 4.6 mm i.d., 5 μm) was purchased from Shimadzu Corporation). The mobile phase consisted of methanol (A) and 0.2% acetic acid (B) of 30:70 (v/v) with the flow rate of 1.0 mL min^{-1} . The injection volume and detection wavelength were 10 μL and 280 nm, respectively. RA and its alkaloids were analyzed by 250 mm \times 4.6 mm, 5 μm C_{18} column (Acchrom Corporation, Liaoning,

China) monitoring at 235 nm. The mobile phase consisted of methanol (A) and 0.2% ammonia solution (B); gradient elution was performed as follows: 0–20 min, 10–30%A; 20–25 min, 30–60%A; 25–45 min, 60–70%A; 45–55 min, 70–90%A; 55–65 min, 90%A.

2.3. Preparation of CMMCNTs

The preparation of high α_{1A} -AR expression HEK 293 cell membrane was conducted as previously described [37]. Briefly, the high α_{1A} -AR expression HEK 293 cells were cultured in DMEM containing 10% fetal bovine serum and supplemented with 100 mg L⁻¹ penicillin, 100 mg L⁻¹ streptomycin, and 300 mg L⁻¹ G418 at 37 °C in 5% CO₂ atmosphere. Then the cells were harvested and washed three times with cold physiological saline (pH 7.4). Cells were following resuspended in hypotonic Tris-HCl (50 mM, pH 7.4) and supersonically ruptured for 30 min. After that, the homogenate was separated by centrifugation at 2000 × g for 10 min at 4 °C, and then the supernatant was collected and centrifuged at 12,000 × g for 20 min at 4 °C. 1 mL physiological saline was subsequently added to the cell membrane pellet.

In the next place, the MCNTs nanomaterials were prepared by a modified chemical coprecipitation method [36] through the electrostatic interaction between MNPs and the surface of CNTs-OH. Briefly, 0.06 g FeCl₃·6H₂O and 0.03 g FeSO₄·7H₂O were dissolved in 80 mL distilled water under sonicating, following ultrasonic dispersion 0.1 g CNTs-OH into the mixed solution for 10 min. After adjusted the pH to 10 by ammonia solution, the mixture was stirred vigorously for 60 min in N₂ atmosphere at 80 °C. Finally, the resultant precipitates were magnetically separated, rinsed thoroughly with ethanol and distilled water for 6 times, and vacuum-dried at 60 °C overnight. For comparison, the bare Fe₃O₄ nanoparticles were prepared through the same process in the absence of CNTs-OH.

Following magnetization of the CNTs-OH, cell membrane camouflaging was performed by fusing sufficiently dispersed MCNTs materials with high α_{1A} -AR expression HEK 293 cell membrane suspension solution under vacuum with ultrasonication for 10 min at 4 °C. After collected the cell membrane-cloaked MCNTs composites by an external magnetic field, the excess cell membrane in supernatant was discarded. Subsequently, a blocking procedure was carried out to prevent non-specific binding, which ensured that the detected signal was directly related to the specific receptor-ligand interaction. In this experiment, the cell membrane-cloaked MCNTs composites were blocked by dispersing in an aqueous solution of BSA (0.5%) and sonicating at 4 °C for 10 min to produce CMMCNTs. As a comparison, non-cell membrane coated MCNTs (NMMCNTs) and native HEK 293 cell membrane coated MCNTs (N-CMMCNTs) were prepared by the same procedure in the absence of cell membrane.

2.4. Confocal microscopy

The CMMCNTs can be imaged by Leica TCS SP5 confocal microscope. Briefly, the prepared CMMCNTs materials were treated with DiI as cell membrane lipid bilayer label. The DiI solution was mixed with CMMCNTs at 4 °C in the dark for 40 min. Then the mixture was washed with PBS buffer three times in order to get rid of excess fluorescent dye. Meanwhile, the fluorescence labeling process of NMMCNTs was the same procedure described above. After that, the LSCM procedure was conducted. The excitation wavelength and emission wavelength of DiI imaging was 549 and 565 nm, respectively. The DiI labeled cell membrane should be observed with significant red fluorescence.

2.5. Binding experiments

To evaluate the adsorption performance of obtained materials, static adsorption, dynamic adsorption, and selective adsorption experiments were performed. Tamsulosin, the first subtype-selective (α_{1A}) α_1 -adrenoceptor antagonist, was used as positive medicine to perform all

the experiments [38,39]. The adsorption capacity was calculated as Eq. (1):

$$Q = (C_0 - C_e)V/m \quad (1)$$

where C_0 and C_e (mg mL⁻¹) represent the initial and equilibrium concentrations of analyte solution, respectively. V (mL) is the volume of analyte solution, m (mg) is the weight of adsorbent, and Q (mg g⁻¹) represents the amount of analyte bounded by adsorbent.

In order to obtain the maximum adsorption capacity of synthesized CMMCNTs, NMMCNTs, and N-CMMCNTs, adsorption isotherm experiments were conducted by adding 5 mg composites into 1 mL tamsulosin solution with different concentrations ranging from 10 to 3000 mg L⁻¹, respectively. Followed ultrasonic dispersion for 1 min, the mixture was subjected to incubate at 37 °C for 30 min, and then the residual tamsulosin in supernatant was measured by HPLC.

For the adsorption kinetics tests, 5 mg CMMCNTs, NMMCNTs, or N-CMMCNTs were added into 1 mL tamsulosin solution (100 mg L⁻¹), which was then incubated at a pre-set time interval from 0.16 to 30 min. After that, the residual tamsulosin in supernatant was quantitatively analyzed by HPLC.

In addition, the selectivity tests were performed to evaluate the specific binding ability of CMMCNTs, NMMCNTs, and N-CMMCNTs toward five drugs (tamsulosin, silodosin, nitrendipine, metoprolol, and verapamil) which act on different receptors. Briefly, the experiment was conducted by adding 5 mg CMMCNTs, NMMCNTs, or N-CMMCNTs into 1 mL each standard solution (100 mg L⁻¹) individually, and the following procedure was then conducted as described earlier in static adsorption experiments.

2.6. Extraction of active compounds from RA

A series of extraction, filtration, and concentration steps were conducted to prepare the total extract. In short, 15 g RA was smashed to powder, prior to extracted by refluxing in 150 mL 70% ethanol at 65 °C for 2 h. Then the filtrate was condensed to dryness by rotary evaporator at 60 °C, and the obtained total extract was stored at -20 °C before use.

For SPE analysis, the RA total extract was dissolved in distilled water, then 5 mg CMMCNTs were incubated with 1 mL extract solution on a shaker for 10 min at 37 °C. After that, the CMMCNTs were separated by magnet and washed with 0.1% acetic acid, and then the analytes were desorbed from the CMMCNTs with 2 mL 0.5% acetic acid. Finally, all collected solutions were evaporated to dryness and the obtained residue was redissolved in 0.5 mL methanol for HPLC analysis. Each individual sample was prepared in triplicate.

2.7. In vitro vascular ring tension test

Vasodilator responses to lappaconitine and benzoylmesaconine were assessed with isolated rat antral circular smooth muscle strips mounted in isometric myographs (Danish Myograph Technology, DMT) and maintained at 37 °C in physiological Kerb's-Henseleit (K-H) solution, aerating with 95% O₂ and 5% CO₂ continuously. After equilibration with 4 mN resting tension for 60 min, 60 mmol L⁻¹ K⁺-rich K-H solution was added into the bath to detect the activity of vessel rings. The preparations were stimulated twice with K⁺-rich K-H solution and each control K⁺ contraction was followed by three washes with K-H solution that allowed to relax to basal tension. K-H solution in the bath was renewed continuously every 20 min during the experiment. After obtaining a stable platform of contraction, dilation of blood vessels was performed on phenylephrine (PE)-induced rings, following the concentration-dependent relaxation curves of lappaconitine and benzoylmesaconine (10⁻⁸–10⁻⁴ mol L⁻¹).

2.8. Rabbit prostatic smooth muscle tension test

Prostatic smooth muscle was dissected from healthy male New

Zealand white rabbits. After cleaned of fat and connective tissues, the muscle was cut into longitudinal strips ($0.2 \times 0.2 \times 1$ cm) and mounted in DMT isometric myographs maintained at 37°C in physiological K-H solution, aerating with 95% O_2 and 5% CO_2 continuously. The activity of prostatic muscle strips was assessed in DMT isometric myographs as described above. After the initial equilibration, $10\ \mu\text{M}$ PE was added into the bath successively to induce a stable contraction. In this study, the widely used highly potent α_{1A} -AR antagonist tamsulosin was selected as positive control. After obtaining a stable platform of contraction, muscle strips were exposed to the increasing doses of tamsulosin and lappaconitine (10^{-8} – 10^{-4} mol L^{-1}).

2.9. Molecular docking study

For better understanding the binding mode of the bioactive compounds with the active sites of α_{1A} -AR, the molecular docking test was performed using the Surflex-dock program in Sybyl X-2.0 version. The crystal structure of α_{1A} -AR (PDB code: 4iye) was downloaded from the RCSB Protein Data Bank. The 3D-structure of docking compounds tamsulosin, lappaconitine, and benzoylemesaconine were depicted using the Sybyl/Sketch module (Tripos Inc.), followed by the structural energy minimization. An empirical scoring function was employed for molecular docking study.

3. Results and discussion

3.1. Preparation of CMMCNTs

The scheme for preparation of CMMCNTs was depicted in Fig. 1. At first, the adsorption amounts of different functionalized CNTs to cell membrane have been investigated, and the result was depicted in Fig.

S1, showed that CNTs-OH have greater adsorption capacity compared to the other functionalized CNTs. Hence, the CNTs-OH was selected to perform all experiment. In brief, MCNTs were synthesized according to the reported method with a few modifications. In short, the positive iron ions ($\text{FeCl}_3 \cdot 6\text{H}_2\text{O}$ and $\text{FeSO}_4 \cdot 7\text{H}_2\text{O}$) were introduced to the surface of CNTs-OH through electrostatic attraction, and then the Fe_3O_4 was in situ generated by the addition of ammonia. The mass ratio of Fe_3O_4 and CNTs-OH was investigated to obtain adequate magnetism without affecting the surface adsorption sites, which was determined by measuring the membrane bounding amounts and the magnetic response time of corresponding materials in solution. As shown in Fig. S2, the bounding amounts of membrane and magnetic response time were decreased with the increase of mass ratio from 0.6:1 to 3:1 ($\text{FeCl}_3 \cdot 6\text{H}_2\text{O}$: CNTs-OH). It can be concluded that with the increase of mass ratio, aggregations of Fe_3O_4 would reduce the active sites of CNTs-OH, leading to the decrease of bounding amounts of membrane. Although the magnetic response ability has been improved with the increase of mass of Fe_3O_4 , the magnetic response time of 33 s was sufficient for rapid separation. Therefore, the mass ratio of $\text{FeCl}_3 \cdot 6\text{H}_2\text{O}$: CNTs-OH was selected as 0.6:1.

Furthermore, high α_{1A} -AR expression cell membrane camouflaging on the MCNTs was performed by dispersing and fusing 1 mL cell membrane with 5 mg MCNTs materials via a sonication step. In order to obtain more effective CMMCNTs, the concentration of cell membrane protein and incubation time were optimized via examining cell membrane protein amounts of supernatant by BCA protein quant assay kit. Three concentrations of cell membrane of 3000, 5000 and $10000\ \text{mg}\ \text{L}^{-1}$ were investigated, and the optimum concentration for the satisfied adsorption amount of cell membrane protein was $5\ \text{mg}\ \text{mL}^{-1}$ (Table S1). In addition, incubation time of 1, 10 and 60 min were tested. As seen in Table S1, when the time was increased from 1 to

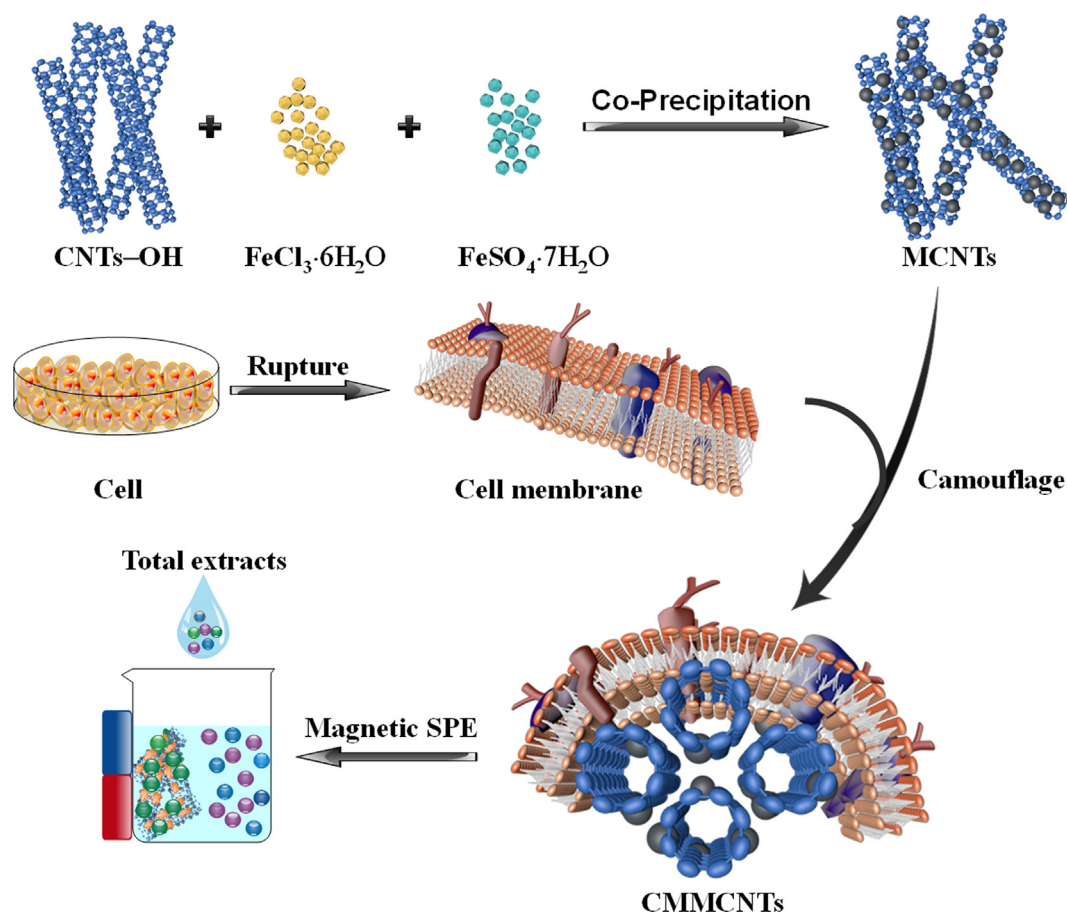


Fig. 1. The schematic illustration of preparation and application of CMMCNTs.

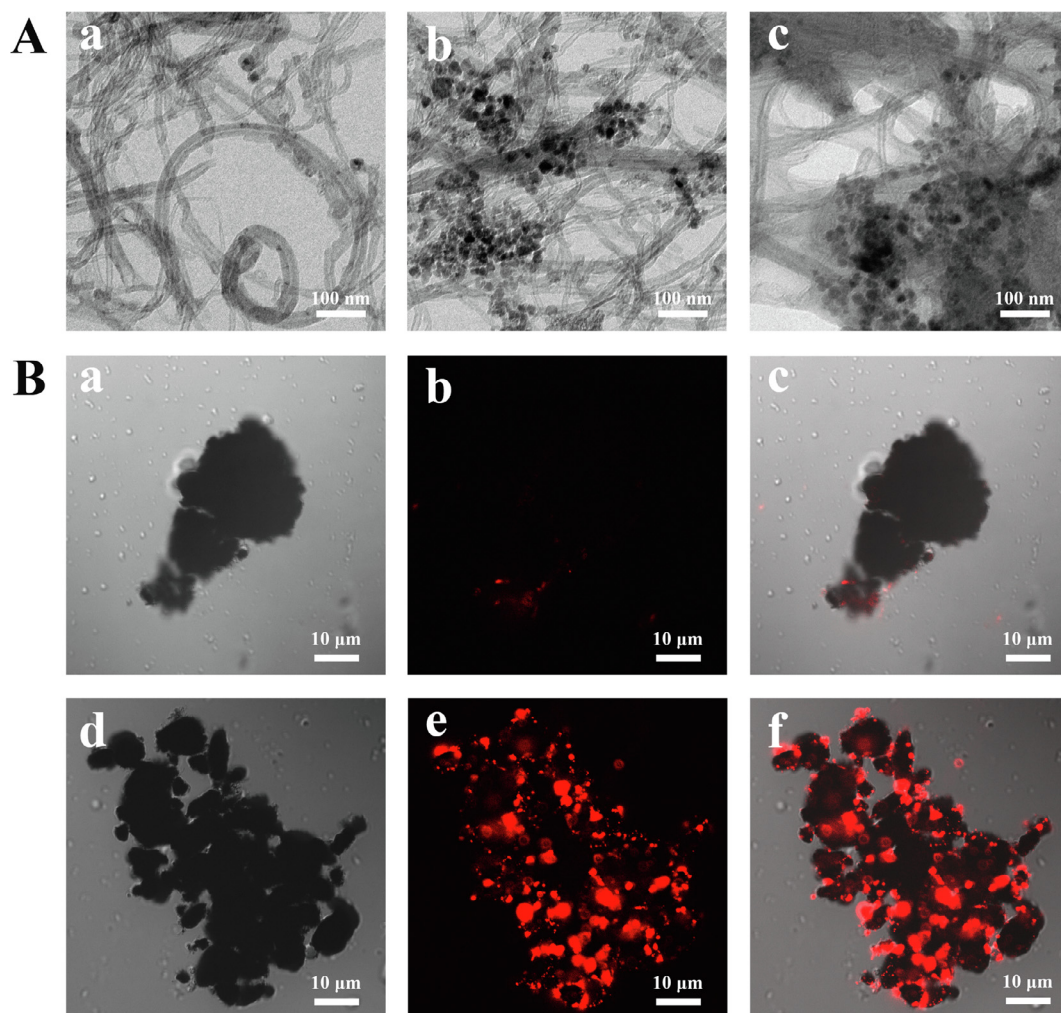


Fig. 2. (A) TEM images of CNTs-OH (a), MCNTs (b), and CMMCNTs (c); (B) LSCM images of MCNTs (a, b, and c) and CMMCNTs (d, e, and f): (a and d) were bright field; (b and e) were excited at 549 nm to observe DiI-dyed cell membrane; (c) were merged by (a) and (b); (f) were merged by (c) and (d).

10 min, MCNTs exhibited rapidly increasing adsorption rate for cell membrane, and then until 60 min, the adsorption amounts remained stable. Therefore, the optimal preparation conditions were found to be the concentration of cell membrane protein of 5000 mg L⁻¹ and incubation time of 10 min.

3.2. Characterization of CMMCNTs

To investigate the morphology of the prepared CMMCNTs composites, TEM images were performed and the results were shown in Fig. 2. Before modification with Fe₃O₄, CNTs-OH with clean and smooth surface was observed in Fig. 2Aa. By contrast, a little of Fe₃O₄ particles were grafted on the surface or edge of the CNTs-OH with a size about 10–30 nm (Fig. 2Ab), which was a clear indication of the decoration of Fe₃O₄ on the CNTs-OH. It was believed that the preparation of MCNTs not only maintained the great adsorption behavior of CNTs-OH but also made it easy to be magnetically separated in applications [8]. After the cell membrane coating process, a thin layer of cell membrane was camouflaged on the surface of MCNTs (Fig. 2Ac), which illustrated a successful decoration of cell membrane on MCNTs.

To further visually validate the coating efficiency, DiI, a typical membrane lipid bilayer dye, was used for cell membrane labeling to evaluate the camouflage of cell membrane on MCNTs. As shown in Fig. 2B, the CMMCNTs (e, f) exhibited obvious red fluorescence in visual field by LSCM imaging and no red fluorescence was detected in MCNTs (b, c), indicating the successful camouflage of membrane lipid

bilayer on the MCNTs.

The prepared composites were expected to possess adequate magnetic properties, which were conducted using VSM at room temperature. Fig. 3A showed the magnetic hysteresis loops of Fe₃O₄ (curve (a)), MCNTs (curve (b)), and CMMCNTs (curve (c)). It can be seen that the magnetic saturation (M_s) values were 70, 50, and 30 emu g⁻¹, respectively. The decrease in M_s values may be attributed to the CNTs-OH decoration and the cell membrane layer coating. These results demonstrated the adequate magnetic response of CMMCNTs, which enabled them to be rapidly separated by placing an external magnetic field.

FTIR spectra of Fe₃O₄, CNTs-OH, and MCNTs were performed to monitor the procedure of the surface functionalization. As shown in Fig. 3B, the peak at 580 cm⁻¹ was the stretching vibration attributed to the interactions of Fe–O–Fe in Fe₃O₄ (curve (a)). As seen from curve (b), the band at 1630 cm⁻¹ was the characteristic graphite structure peak, which was assigned to the C=C groups of the CNTs. In addition, the peaks at 2895 and 2875 cm⁻¹ were attributed to the stretching vibration of C–H, and 3443 cm⁻¹ was assigned to the stretching mode of O–H in the functional groups of the CNTs-OH. Compared with the two spectra (curve (a) and (b)), the coexistence of the characteristic peaks of Fe₃O₄ and CNTs-OH in curve (c) was direct evidence to verify the fabrication of MCNTs.

XPS analysis was carried out to characterize the chemical compositions of CNTs-OH, Fe₃O₄, MCNTs, and CMMCNTs. As shown in Fig. 3C, the peak of Fe 2p in the prepared MCNTs (curve (c)) was

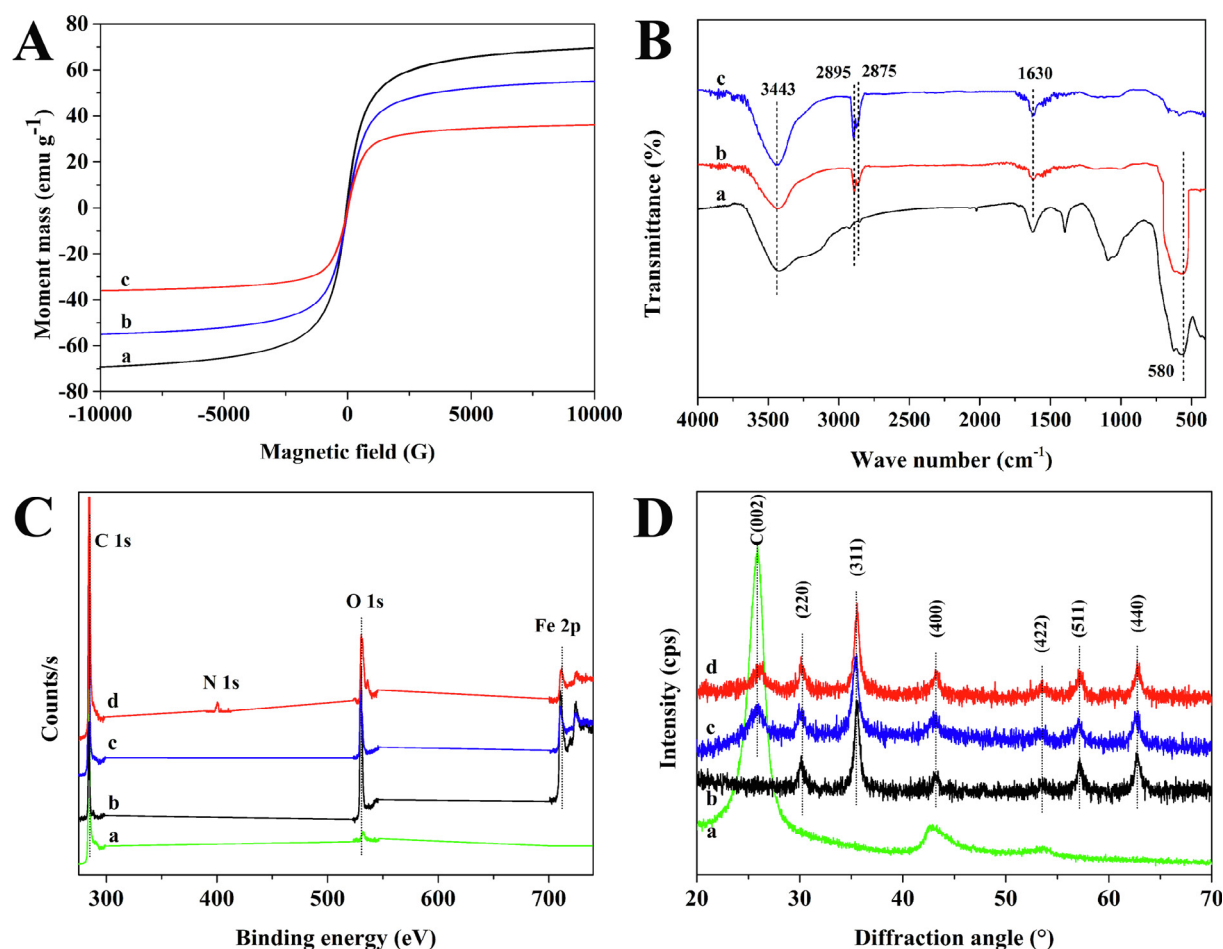


Fig. 3. (A) Magnetic hysteresis loops of Fe₃O₄ (a), MCNTs (b), and CMMCNTs (c); (B) FTIR spectra of Fe₃O₄ (a), CNTs-OH (b), and MCNTs (c); (C) XPS characterization of CNTs-OH (a), Fe₃O₄ (b), MCNTs (c), and CMMCNTs (d); (D) XRD patterns of CNTs-OH (a), Fe₃O₄ (b), MCNTs (c), and CMMCNTs (d).

obviously observed compared with the pristine CNTs-OH (curve (a)) and Fe₃O₄ (curve (b)), which further confirmed that Fe₃O₄ was successfully decorated on CNTs-OH. Moreover, after the camouflage of cell membrane, the N 1 s peak appeared at 400.0 eV in curve (d), which was corresponded to the nitrogen element of the cell membrane, demonstrating the successful formation of CMMCNTs.

The crystal structures and phase compositions of CNTs-OH, Fe₃O₄, MCNTs, and CMMCNTs were further examined by XRD, and the results were presented in Fig. 3D. Clearly, the diffraction peak at 26.4° represented the typical Bragg-peak and can be ascribed to the (002) reflection of CNTs-OH (curve (a)). Besides, six characteristic diffraction peaks ($2\theta = 30.3^\circ, 35.6^\circ, 43.3^\circ, 53.7^\circ, 57.4^\circ, \text{ and } 62.7^\circ$) were observed in curve (b), corresponding to the (220), (311), (400), (422), (511), and (440) planes to Fe₃O₄ (JCPDS No. 65–3107). For the MCNTs (curve (c)) and CMMCNTs (curve (d)), the typical diffraction peaks of CNTs-OH and Fe₃O₄ were appeared together, which confirmed that the CNTs-OH had been successfully decorated with Fe₃O₄ nanoparticles, and the crystallinity of the prepared composites remained unchanged during grafting of Fe₃O₄ and coating of cell membrane.

TGA profiles of Fe₃O₄, CNTs-OH, MCNTs, and CMMCNTs were presented in Fig. S3. CNTs-OH (curve (b)) and MCNTs (curve (c)) lost their weight about 6% as the temperature rose, which may be attributed to the loss of carbon atoms from imperfect regions of the walls of nanotubes, together with some residual water and other impurities [40]. An estimation of the cell membrane proportion in dry CMMCNTs has been made from TGA results (curve (d)), which presented a sharp mass loss about 25% as the temperature increased from 750 °C to 800 °C, corresponding to the decomposition of cell membrane on the surface of

MCNTs. The mass loss values showed the decorating amounts of cell membrane on MCNTs, indicating the successful modification.

3.3. Adsorption capacity

The static adsorption tests of adsorbents with various tamsulosin concentrations (10–3000 mg L⁻¹) were investigated at room temperature. As displayed in Fig. 4A, with the increase of the concentration of tamsulosin, the adsorption capacity of all adsorbents increased progressively and then reached equilibrium at the concentration of 1000 mg L⁻¹. Besides, the saturated adsorption amounts of CMMCNTs, NMMCNTs, and N-CMMCNTs were 73.1, 13.2, and 13.4 mg g⁻¹, respectively. The experimental results proved that the saturated adsorption capacity of CMMCNTs was much higher than those of NMMCNTs and N-CMMCNTs at the same condition. In other words, the high α_{1A} -AR expression HEK 293 cell membrane cloaking provided MCNTs with more ligand recognition sites, as a result, exhibiting great potential in biological recognition and adsorption.

To further estimate the bounding properties of CMMCNTs, NMMCNTs, and N-CMMCNTs, the Langmuir, Freundlich, Dubinin-Radushkevich, and Scatchard isotherms were used to analyze the static adsorption experiments data, respectively. All parameters were compiled in Table 1, the correlation coefficient (r) of the Langmuir model of CMMCNTs, NMMCNTs, and N-CMMCNTs were 0.9947, 0.9650, and 0.9946, respectively, which were greater than those of the other three models. This result showed that the Langmuir model fitted the adsorption data better than the others, indicating a monolayer adsorption occurred on a homogeneous surface of the prepared materials [41].

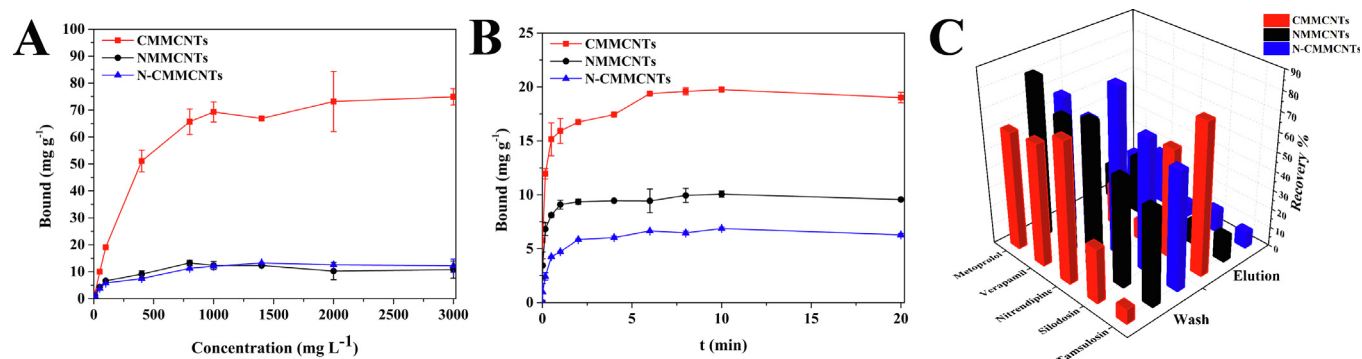


Fig. 4. (A) Static adsorption isotherm curves, (B) dynamic adsorption curves, and (C) adsorption selectivity results of CMMCNTs, NMMCNTs, and N-CMMCNTs.

The essential features of the Langmuir isotherm model can be evaluated using separation factor constant R_L (dimensionless), which can be defined as Eq. (2):

$$R_L = \frac{1}{1 + K_L C_m} \quad (2)$$

where C_m (mg L^{-1}) is the maximum initial concentration of tamsulosin. The smaller R_L is, the adsorbent is more favorable for tamsulosin. R_L of NMMCNTs and N-CMMCNTs were 0.0979 and 0.0723, respectively, which were much less than that of CMMCNTs (0.1231), indicating that the adsorption effect of CMMCNTs was better than NMMCNTs and N-CMMCNTs.

3.4. Adsorption kinetics

To evaluate the adsorption kinetics of the adsorbents, the influence of incubation time on the adsorption amounts of the materials was estimated. It can be inferred from Fig. 4B, as the time increased, the adsorption amounts of tamsulosin for all three adsorbents increased sharply at the initial phase, and then approaching equilibrium slowly within 5 min. The adsorption amounts of CMMCNTs was much higher than that of NMMCNTs and N-CMMCNTs. These results demonstrated that the surface of CMMCNTs possessed amounts of cell membrane receptor sites that could be accessed by positive drugs with less resistance.

In order to further evaluate the kinetic mechanism of adsorption process, two kinds of the most widely used kinetic models, pseudo-first-order and pseudo-second-order equations (Eqs. (3) and (4)), were

applied to fit the data.

$$\ln(Q_e - Q_t) = \ln Q_e - k_1 t \quad (3)$$

$$\frac{t}{Q_t} = \frac{1}{k_2 Q_e^2} + \frac{t}{Q_e} \quad (4)$$

where Q_e (mg g^{-1}) is the actual amount of tamsulosin adsorbed at equilibrium, and Q_t (mg g^{-1}) is the adsorption amount of tamsulosin at time t (min). k_1 (min^{-1}) and k_2 ($\text{g mg}^{-1} \text{min}^{-1}$) are the rate constants of pseudo-first-order and pseudo-second-order models, respectively. The corresponding parameters were summarized in Table S2.

It was obvious that the r values of pseudo-second-order model of CMMCNTs, NMMCNTs, and N-CMMCNTs were 0.9783, 0.9883, and 0.9912, respectively, which were higher than those of pseudo-first-order (0.9516, 0.9617, and 0.9784). This result implied that the adsorption process was confirmed to pseudo-second-order model perfectly. Therefore, the adsorption process was attributed to chemical adsorption, which could be related to the hydrogen bond between medicine and receptor [42].

3.5. Adsorption selectivity

The selective recognition toward active compounds was an important property for preparation of CMMCNTs. Herein, tamsulosin and silodosin blocking the α_{1A} -AR were chosen as positive drugs. Nitrendipine, metoprolol, and verapamil acting on different kinds of receptors were used as negative drugs. The adsorption amounts of CMMCNTs, NMMCNTs, and N-CMMCNTs for five drugs were presented

Table 1

Equations and parameters of adsorption isotherms of CMMCNTs, NMMCNTs, and N-CMMCNTs.

Isotherm model	Equation and parameters	CMMCNTs	NMMCNTs	N-CMMCNTs
Freundlich	$\lg Q_e = \lg K_F + m \lg C_e$			
	K_F (L mg^{-1})	0.7560	0.7834	0.5782
	m	0.6315	0.3785	0.4236
	r	0.8938	0.9589	0.9513
Langmuir	$\frac{C_e}{Q_e} = \frac{1}{Q_{\max} K_L} + \frac{1}{Q_{\max}} C_e$			
	K_L (L mg^{-1})	0.0036	0.0115	0.0092
	Q_{\max} (mg g^{-1})	88.50	9.64	12.67
	r	0.9940	0.9650	0.9946
Dubinin-Radushkevich	$\lg T_e = \lg T_{\max} - K_{ad} \left(RT \lg \left(1 + \frac{1}{C_e} \right) \right)^2$			
	K_{ad} ($\text{mg}^2 \text{kJ}^{-2}$)	5.5×10^{-5}	3.7×10^{-5}	4.0×10^{-5}
	Q_s (mg g^{-1})	51.63	10.08	9.22
	r	0.8235	0.8992	0.8863
Scatchard	$\frac{Q_e}{C_e} = \frac{Q_{\max} - Q_e}{K_d}$			
	K_d (mg L^{-1})	396.83	125.60	131.58
	Q_{\max} (mg g^{-1})	89.97	13.87	13.18
	r	0.9680	0.9366	0.9807

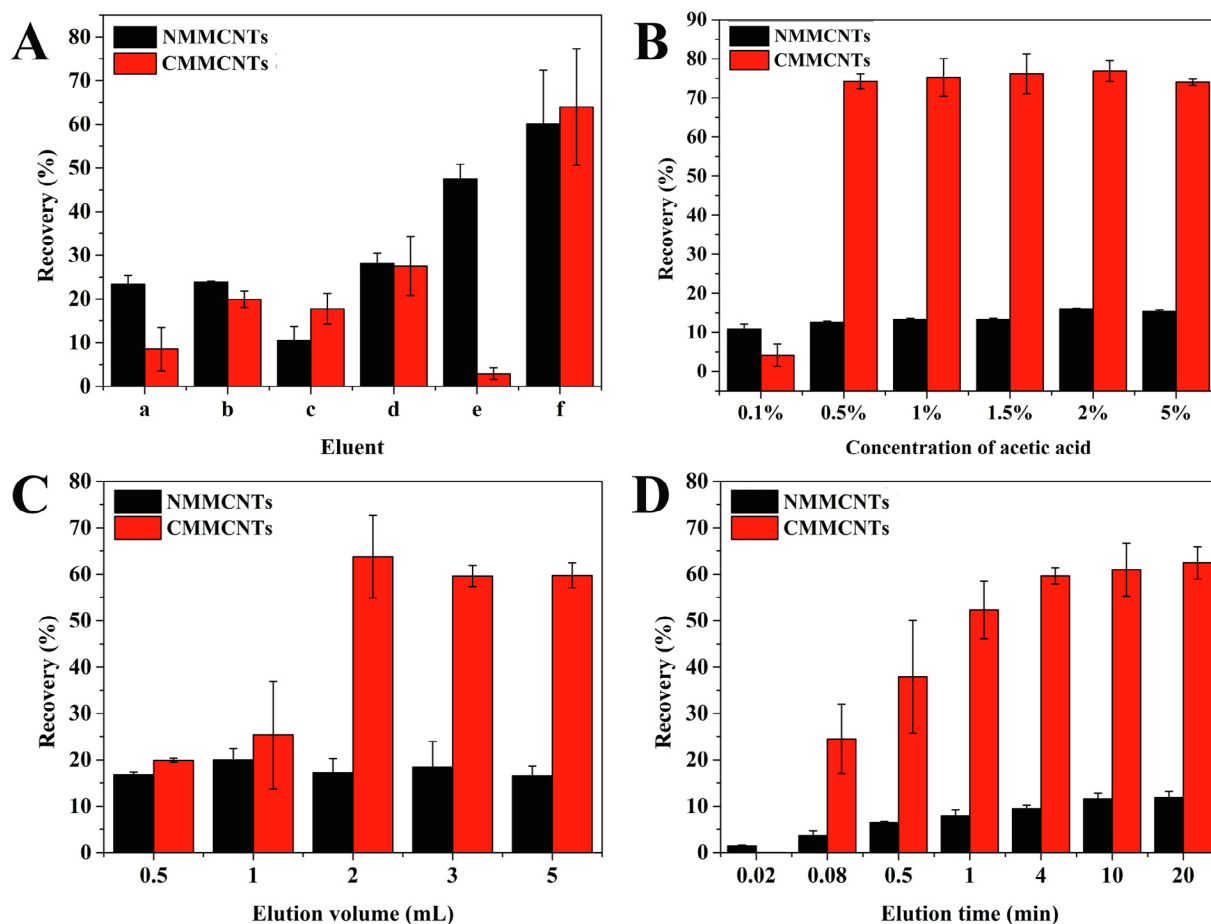


Fig. 5. Optimization of SPE procedure. (A) Selection of washing solvent: (a) water, (b) PBS, (c) PBS-isopropanol mixture (7:3, v/v), (d) PBS-isopropanol mixture (5:5, v/v), (e) 0.1% acetic acid, and (f) 0.5% acetic acid; (B) Selection of elution solvent; (C) Elution volume; (D) Elution time.

in Fig. S4. NMMCNTs and N-CMMCNTs exhibited similar affinity for all drugs, while CMMCNTs showed apparently higher affinity for tamsulosin and silodosin. As can be seen in Fig. 4C, the adsorbed components of NMMCNTs and N-CMMCNTs can be almost completely eluted during the washing process, which can be attributed to nonspecific interactions between NMMCNTs and N-CMMCNTs with the drugs. However, for CMMCNTs, only 7.8% and 28.3% of tamsulosin and silodosin were desorbed during the washing process, respectively, indicating that the specific binding sites were formed by the coating of cell membrane.

3.6. Optimization of SPE procedure

For achieving the optimal extraction efficiency of target analytes, various SPE operating parameters needed to be optimized. In this section, the type of washing solvent, the concentration of acetic acid, elution solvent volume, and elution time were investigated.

The type of washing solvent was crucial for SPE procedure. In this study, different kinds of solvents including water, phosphate buffer saline (PBS), PBS-isopropanol mixture (7:3, v/v), PBS-isopropanol mixture (5:5, v/v), 0.1% acetic acid, and 0.5% acetic acid were investigated. As can be seen in Fig. 5A, 0.1% acetic acid (curve (e)) provided a good cleaning performance, which exhibited excellent desorption efficiency for NMMCNTs but only a weak effect on CMMCNTs. Consequently, 0.1% acetic acid was selected as washing solvent for further experiments.

To achieve high recovery of tamsulosin, the elution step was an important process to ensure that the adsorbates were completely desorbed. On account of acid has a good effect on disrupting the interactions between the drugs and receptors, the concentration of acetic acid

was investigated varied from 0.1% to 5.0%. Fig. 5B showed that the maximum amounts of tamsulosin were eluted when concentration of the acetic acid was adjusted at 0.5%. And as the concentration further increased, the recovery was no longer changed. As a result, 0.5% acetic acid was chosen as the optimum eluent in the subsequent experiments.

Moreover, the effect of the elution solvent volume was studied in the interval of 0.5–5 mL (Fig. 5C). The results demonstrated that 2 mL 0.5% acetic acid solution was sufficient to achieve satisfactory recovery, and with the volume further increased, the recovery did not change significantly. Accordingly, 2 mL was chosen as the volume of desorption solvent for further experiments.

In addition, to determine the optimum desorption time, elution time between 0.02 and 20 min was employed under ultrasonication. As shown in Fig. 5D, the desorption efficiency on CMMCNTs increased rapidly with the increase of elution time and reached maximum at 4 min with no further apparent change until 20 min. Based on the results, 4 min was selected as the elution time for the subsequent experiments.

3.7. Method validation

Analytical parameters of the proposed SPE method, where the obtained CMMCNTs composites were applied as adsorbents, were validated under the optimized experiment conditions. Triplicate experiments were carried out for all the evaluations. Good linearity was obtained for tamsulosin between 1 and 1000 mg L⁻¹ with *r* of 0.9997. The limit of detection (LOD) was determined with signal-to-noise ratio of 3:1 and detected as 0.8 mg L⁻¹.

In order to access the repeatability of the method, intra-day and

Table 2
The recovery of tamsulosin in three concentration levels in RA.

Analyte	50 mg L ⁻¹		500 mg L ⁻¹		1000 mg L ⁻¹	
	Recovery (%)	RSD (%)	Recovery (%)	RSD (%)	Recovery (%)	RSD (%)
Tamsulosin	56.5	13.9	65.7	10.6	75.2	5.0

inter-day precisions were evaluated by six consecutive measurements of samples within one day and for six days, respectively. The results showed that relative standard deviation (RSD) of intra-day and inter-day were 1.4% and 2.2%, respectively, which demonstrated the good precision of the method. Besides, the reproducibility of six batches of adsorbents were investigated, the RSD of the recoveries was calculated as 1.6%, indicating the good reproducibility of the SPE method. Moreover, six adsorption-desorption cycles were conducted to investigate the reusability of CMMCNTs. The result showed that after five cycles the adsorption capacity declined sharply with 38.6%, which possibly due to the falling off of cell membrane during the repeated washing and eluting process.

In addition, the standard addition method was performed to further evaluate the accuracy of the SPE method in actual sample analysis. Briefly, the RA extraction were spiked with tamsulosin at three concentration levels (50, 500, and 1000 mg L⁻¹). Based on Table 2, the values of recovery ranging from 56.5% to 75.2% with the RSD values lower than 15.0%. Therefore, the results confirmed the feasibility of the developed SPE methods.

3.8. Application in TCM samples

After fully optimized and validated, the prepared CMMCNTs were applied to screen potential bioactive components from the extraction of RA. The typical chromatograms of the initial extraction solution of RA, the extract after being absorbed by CMMCNTs, the solution after washing, and the elution of adsorbed molecules were displayed in Fig. 6. It could be seen that after adsorption by CMMCNTs, many noninteracting compounds were barely retained and almost diminished (curve (b)), meanwhile other nonspecific bounding compounds were nearly discarded after washing step using 0.1% acetic acid (curve (c)). Regarding to the chromatogram in curve (d), two significant peaks were detected in the elution, which were supposed to active components recognized and enriched from the extraction of RA using CMMCNTs.

In addition, these two compounds were preliminarily identified by TOFMS. As shown in Fig. 6, peaks 1 and 2 corresponded to benzoylmesaconine and lappaconitine, respectively. Then, the standard solution of benzoylmesaconine and lappaconitine were used to verify the inference using HPLC-TOFMS, and the results showed that their MS data were in accordance with peaks 1 and 2, respectively. Therefore,

the results confirmed that CMMCNTs can be used to effectively screen and enrich potential active components acting on specific α_{1A} -AR from TCM.

3.9. Pharmacological effect

In order to preliminarily validate the specific effects of lappaconitine and benzoylmesaconine on α_{1A} -AR, isolated vascular ring tension assay was performed and the results were depicted in Fig. 7A. As a matter of fact, we noticed that lappaconitine showed a significant vasodilatation effect, with the maximum effect (E_{max}) and pEC_{50} values (negative log of median effective concentration) were 97 ± 8.0 (%) and 4.918, respectively. Whereas, benzoylmesaconine with a lower E_{max} approximately 58 ± 7.0 (%), exhibited a weak biological activity, which indicated that lappaconitine could be the bioactive compounds acting on α_{1A} -AR.

Motivated by the above results, the potential bioactive compound lappaconitine was further examined for their affinity for α_{1A} -AR in isolated rabbit prostate with tamsulosin as positive control. As shown in Fig. 7B, tamsulosin and lappaconitine both displayed concentration-dependent relaxing effects on rabbit prostate smooth muscle strips pre-contracted by PE. Although pEC_{50} value of lappaconitine (4.125) was lower than that of tamsulosin (7.266), the maximum relaxation effect induced by lappaconitine was similar to tamsulosin, indicating that lappaconitine has a slow, mild, and persistent relaxation effect on prostate smooth muscle compared to tamsulosin. It could be inferred that lappaconitine still need further structural modification to obtain higher bioactivity and satisfactory clinical effect. Nevertheless, we should highlight that the proposed method was reliable and efficient.

3.10. Interaction simulations of screened alkaloids with α_{1A} -AR

To shed light on the interaction mode with α_{1A} -AR, benzoylmesaconine and lappaconitine were docked into the Ligand binding domains (LBDs) of α_{1A} -AR. Tamsulosin was selected to define the binding cavity. The molecular docking results suggested that the bounding modes of lappaconitine (Fig. S5B) and benzoylmesaconine (Fig. S5C) with the LBDs of α_{1A} -AR were essentially similar to tamsulosin (Fig. S5A). As we can see, lappaconitine formed five hydrogen bonds in the α_{1A} -AR LBDs with Asp37, Lys26, Arg28, Arg40, and Ser38 sites, showed better

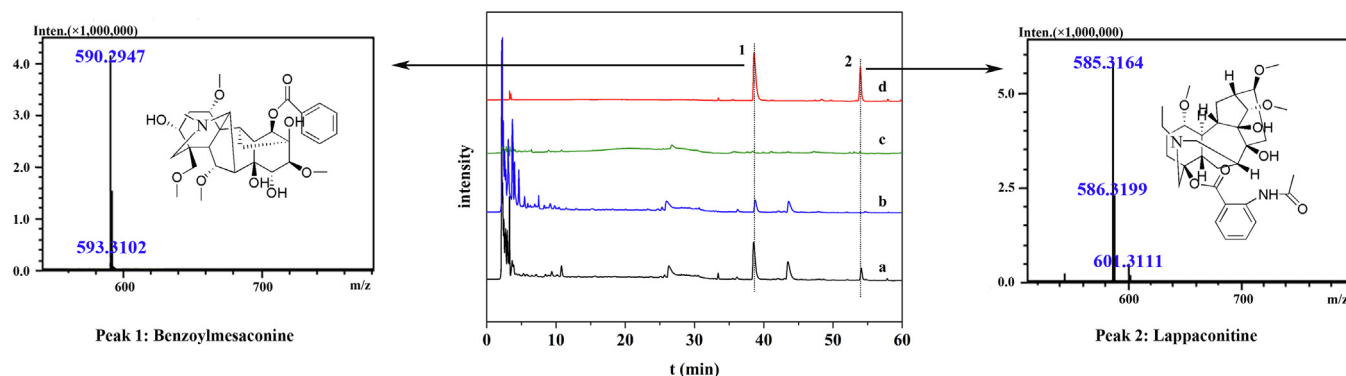


Fig. 6. Chromatograms of the RA extracts. (a) Initial solutions before CMMCNTs extraction, (b) solution after loading, (c) solution after washing, and (d) solution after eluting and TOFMS results of the peak 1 and peak 2.

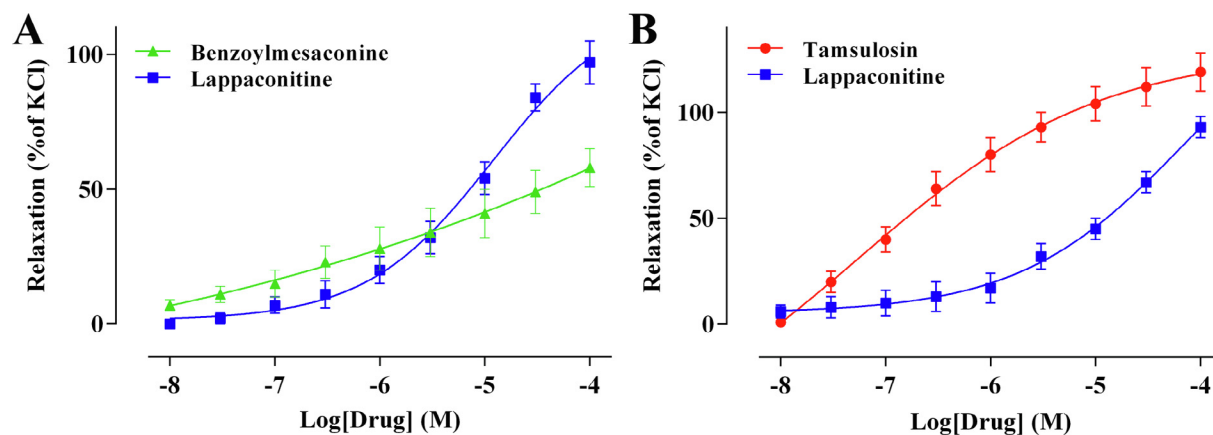


Fig. 7. Concentration-response curves of PE-induced contractions in (A) rat antral circular smooth muscle strips and (B) isolated rabbit prostate.

hydrogen bonding than benzoylmesaconine. In addition, the total docking score of tamsulosin, lappaconitine, and benzoylmesaconine were 3.7771, 4.2907, and 2.4354, respectively, in agreement with the above pharmacological validate results.

4. Conclusions

In a word, we demonstrated a novel drug discovery platform based on cell membrane-camouflaging MCNTs to effectively target and separate potential active compounds. Specifically, CNTs-OH were decorated with Fe_3O_4 through a facile method, and followed by incorporation with high expression α_{1A} -AR HEK 293 cell membrane using a nondisruptive cloaking protocol. Due to the combination of MCNTs and bioactive cell membrane, the prepared CMMCNTs exhibited high binding capacity, satisfactory selectivity, and rapid separation ability. As a result, two compounds (benzoylmesaconine and lappaconitine) were screened and identified from RA extracts, where lappaconitine showed favorable antagonism to α_{1A} -AR in preliminary pharmacological validation. The successful application showed potential value in specific recognition and separation of active components. Therefore, this strategy was expected to provide a promising platform for drug discovery while open up a novel method for the functionalization of CNTs.

Acknowledgments

This research was supported by the National Natural Science Foundation of China (No. 81503033 and 81673398), the Fundamental Research Funds for the Central Universities (No. xjj2018222), and the Natural Science Foundation of Shaanxi Province (No. 2016JQ8016).

Appendix A. Supplementary data

Supplementary data to this article can be found online at <https://doi.org/10.1016/j.cej.2019.01.171>.

References

- C. Basheer, A. Ainedhary, B. Rao, S. Valliyaveetil, H. Lee, Development and application of porous membrane-protected carbon nanotube micro-solid-phase extraction combined with gas chromatography/mass spectrometry, *Anal. Chem.* 78 (2006) 2853–2858.
- S. Hong, J. Lee, K. Do, M. Lee, J. Kim, S. Lee, D. Kim, Stretchable electrode based on laterally combed carbon nanotubes for wearable energy harvesting and storage devices, *Adv. Funct. Mater.* 27 (2017) 1704354.
- Y. Si, J. Park, S. Jung, G. Hwang, E. Goh, H. Lee, Layer-by-layer electrochemical biosensors configuring xanthine oxidase and carbon nanotubes/graphene complexes for hypoxanthine and uric acid in human serum solutions, *Biosens. Bioelectron.* 121 (2018) 265–271.
- Y. Miao, H. Zhang, Y. Pan, J. Ren, M. Ye, F. Xia, R. Huang, Z. Lin, S. Jiang, Y. Zhang, S. Zhou, Y. Zhang, Single-walled carbon nanotube: one specific inhibitor of cancer stem cells in osteosarcoma upon downregulation of the TGF beta 1 signaling, *Biomaterials* 149 (2017) 29–40.
- M. Valcarcel, S. Cardenas, B.M. Simonet, Y. Moliner-Martinez, R. Lucena, Carbon nanostructures as sorbent materials in analytical processes, *Trend. Anal. Chem.* 27 (2008) 34–43.
- H. Arami, A. Khandhar, D. Liggitt, K.M. Krishnan, In vivo delivery, pharmacokinetics, biodistribution and toxicity of iron oxide nanoparticles, *Chem. Soc. Rev.* 44 (2015) 8576–8607.
- D. Reddy, Y. Yun, Spinel ferrite magnetic adsorbents: Alternative future materials for water purification, *Coordin. Chem. Rev.* 315 (2016) 90–111.
- C. Herrero-Latorre, J. Barciela-García, S. García-Martín, R.M. Pena-Creciente, J. Otarola-Jimenez, Magnetic solid-phase extraction using carbon nanotubes as sorbents: a review, *Anal. Chim. Acta* 892 (2015) 10–26.
- H. Niu, Y. Wang, X. Zhang, Z. Meng, Y. Cai, Easy synthesis of surface-tunable carbon-encapsulated magnetic nanoparticles: adsorbents for selective isolation and preconcentration of organic pollutants, *ACS Appl. Mater. Inter.* 4 (2012) 286–295.
- N. Wang, S. Pandit, L. Ye, M. Edwards, V. Mokkalapati, M. Murugesan, V. Kuzmenko, C. Zhao, F. Westerlund, I. Mijakovic, J. Liu, Efficient surface modification of carbon nanotubes for fabricating high performance CNT based hybrid nanostructures, *Carbon* 111 (2017) 402–410.
- F. Coa, M. Strauss, Z. Clemente, L. Neto, J. Lopes, R. Alencar, A. Souza, O. Alves, V. Castro, E. Barbieri, D. Martinez, Coating carbon nanotubes with humic acid using an eco-friendly mechanochemical method: application for Cu(II) ions removal from water and aquatic ecotoxicity, *Sci. Total Environ.* 607 (2017) 1479–1486.
- M. Valcarcel, S. Cardenas, B.M. Simonet, Role of carbon nanotubes in analytical science, *Anal. Chem.* 79 (2007) 4788–4797.
- L. Liang, W. Xie, S. Fang, F. He, B. Yin, C. Tlili, D. Wang, S. Qiu, Q. Li, High-efficiency dispersion and sorting of single-walled carbon nanotubes via non-covalent interactions, *J. Mater. Chem. C* 5 (2017) 11339–11368.
- M. Ata, R. Poon, A. Syed, J. Milne, I. Zhitomirsky, New developments in non-covalent surface modification, dispersion and electrophoretic deposition of carbon nanotubes, *Carbon* 130 (2018) 584–598.
- M. Kawamoto, P. He, Y. Ito, Green processing of carbon nanomaterials, *Adv. Mater.* 29 (2017) 1602423.
- W. Zhu, Y. Li, L. Dai, J. Li, X. Li, W. Li, T. Duan, J. Lei, T. Chen, Bioassembly of fungal hyphae/carbon nanotubes composite as a versatile adsorbent for water pollution control, *Chem. Eng. J.* 339 (2018) 214–222.
- R. Fang, A. Kroll, W. Gao, L. Zhang, Cell membrane coating nanotechnology, *Adv. Mater.* 30 (2018) 1706759.
- J. Green, J. Elisseeff, Mimicking biological functionality with polymers for biomedical applications, *Nature* 540 (2016) 386–394.
- Q. Fu, P. Lv, Z. Chen, D. Ni, L. Zhang, H. Yue, Z. Yue, W. Wei, G. Ma, Programmed co-delivery of paclitaxel and doxorubicin boosted by camouflaging with erythrocyte membrane, *Nanoscale* 7 (2015) 4020–4030.
- C. Hu, L. Zhang, S. Aryal, C. Cheung, R. Fang, L. Zhang, Erythrocyte membrane-camouflaged polymeric nanoparticles as a biomimetic delivery platform, *Proc. Natl. Acad. Sci. U.S.A.* 108 (2011) 10980–10985.
- H. Chen, Z. Fang, Y. Chen, Y. Chen, B. Yao, J. Cheng, C. Chien, Y. Chang, C. Hu, Targeting and enrichment of viral pathogen by cell membrane cloaked magnetic nanoparticles for enhanced detection, *ACS Appl. Mater. Inter.* 9 (2017) 39953–39961.
- W. Liu, M. Ruan, Y. Wang, R. Song, X. Ji, J. Xu, J. Dai, W. Xue, Light-triggered biomimetic nanoerythrocyte for tumor-targeted lung metastatic combination therapy of malignant melanoma, *Small* 14 (2018) e1801754.
- Z. Wu, T. Li, W. Gao, T. Xu, B. Jurado-Sanchez, J. Li, W. Gao, Q. He, L. Zhang, J. Wang, Cell-membrane-coated synthetic nanomotors for effective biodegradation, *Adv. Funct. Mater.* 25 (2015) 3881–3887.
- Z. Chen, P. Zhao, Z. Luo, M. Zheng, H. Tian, P. Gong, G. Gao, H. Pan, L. Liu, A. Ma, H. Cui, Y. Ma, L. Cai, Cancer cell membrane-biomimetic nanoparticles for homologous-targeting dual-modal imaging and photothermal therapy, *ACS Nano* 10 (2016) 10049–10057.

- [25] F. Cheung, TCM made in China, *Nature* 480 (2011) S82–S83.
- [26] X. Mao, D. Kaufman, C. Crowder, Nicotinamide mononucleotide adenylyl-transferase promotes hypoxic survival by activating the mitochondrial unfolded protein response, *Cell Death Dis.* 7 (2016) e2113.
- [27] T. Isah, A. Mujib, Camptothecin from *Nothapodytes nimmoniana*: review on biotechnology applications, *Acta Physiol. Plant.* 37 (2015) 106.
- [28] H. Luo, L. Chen, Z. Li, Z. Ding, X. Xu, Frontal immunoaffinity chromatography with mass spectrometric detection: a method for finding active compounds from traditional Chinese herbs, *Anal. Chem.* 75 (2003) 3994–3998.
- [29] X. Chen, Y. Cao, H. Zhang, Z. Zhu, M. Liu, H. Liu, X. Ding, Z. Hong, W. Li, D. Lv, L. Wang, X. Zhuo, J. Zhang, X. Xie, Y. Chai, Comparative normal/failing rat myocardium cell membrane chromatographic analysis system for screening specific components that counteract doxorubicin-induced heart failure from *aconitum carmichaeli*, *Anal. Chem.* 86 (2014) 4748–4757.
- [30] X. Ding, Y. Cao, Y. Yuan, Z. Gong, Y. Liu, L. Zhao, L. Lv, G. Zhang, D. Wang, D. Jia, Z. Zhu, Z. Hong, X. Chen, Y. Chai, Development of APTES-decorated HepG2 cancer stem cell membrane chromatography for screening active components from *salvia miltiorrhiza*, *Anal. Chem.* 88 (2016) 12081–12089.
- [31] X. Chen, Y. Cao, D. Lv, Z. Zhu, J. Zhang, Y. Chai, Comprehensive two-dimensional HepG2/cell membrane chromatography/monolithic column/time-of-flight mass spectrometry system for screening anti-tumor components from herbal medicines, *J. Chromatogr. A* 1242 (2012) 67–74.
- [32] Y. Bu, Q. Hu, R. Ke, Y. Sui, X. Xie, S. Wang, Cell membrane camouflaged magnetic nanoparticles as a biomimetic drug discovery platform, *Chem. Comm.* 54 (2018) 13427–13430.
- [33] J.R. Docherty, Subtypes of functional alpha 1-adrenoceptor, *Cell. Mol. Life Sci.* 67 (2010) 405–417.
- [34] M. Rosini, M.L. Bolognesi, D. Giardina, A. Minarini, V. Tumiatti, C. Melchiorre, Recent advances in alpha(1)-adrenoceptor antagonists as pharmacological tools and therapeutic agents, *Curr. Top. Med. Chem.* 7 (2007) 147–162.
- [35] R. Kumar, P. Malla, M. Kumar, Advances in the design and discovery of drugs for the treatment of prostatic hyperplasia, *Expert Opin. Drug Dis.* 8 (2013) 1013–1027.
- [36] G. Morales-Cid, A. Fekete, B.M. Simonet, R. Lehmann, S. Cardenas, X. Zhang, M. Valcarcel, P. Schmitt-Kopplin, In situ synthesis of magnetic multiwalled carbon nanotube composites for the clean-up of (fluoro)quinolones from human plasma prior to ultrahigh pressure liquid chromatography analysis, *Anal. Chem.* 82 (2010) 2743–2752.
- [37] S. Han, T. Zhang, L. Feng, N. Lv, S. Wang, Screening of target compounds from *Fructus Piperis* using high alpha(1A) adrenoceptor expression cell membrane chromatography online coupled with high performance liquid chromatography tandem mass spectrometry, *J. Pharmaceut. Biomed.* 81–82 (2013) 133–137.
- [38] M. Wilde, D. McTavish, Tamsulosin A review of its pharmacological properties and therapeutic potential in the management of symptomatic benign prostatic hyperplasia, *Drugs* 52 (1996) 883–898.
- [39] O. Ukimura, M. Kanazawa, A. Fujihara, K. Kamoi, K. Okihara, T. Miki, Naftopidil versus tamsulosin hydrochloride for lower urinary tract symptoms associated with benign prostatic hyperplasia with special reference to the storage symptom: A prospective randomized controlled study, *Int. J. Urol.* 15 (2008) 1049–1054.
- [40] H. Hosseinzadeh, S. Pashaei, S. Hosseinzadeh, Z. Khodaparast, S. Ramin, Y. Saadat, Preparation of novel multi-walled carbon nanotubes nanocomposite adsorbent via RAFT technique for the adsorption of toxic copper ions, *Sci. Total Environ.* 640 (2018) 303–314.
- [41] J. Zhang, X. Yan, X. Hu, R. Feng, M. Zhou, Direct carbonization of Zn/Co zeolitic imidazolate frameworks for efficient adsorption of Rhodamine B, *Chem. Eng. J.* 347 (2018) 640–647.
- [42] J. Tang, Y. Li, X. Wang, M. Daroch, Effective adsorption of aqueous Pb²⁺ by dried biomass of *landoltia punctata* and *spirodela polyrhiza*, *J. Clean. Prod.* 145 (2017) 25–34.